

# Effects of the Post-Deposition Annealing Treatment on the Electrochemical Behavior of TiN Coatings Deposited by CAE-PVD Method

Yemurai Vengesa, Arash Fattah-alhosseini\*, Hassan Elmkhah, Omid Imantalab

\* a.fattah@basu.ac.ir

\* Department of Materials Engineering, Bu-Ali Sina University, Hamedan, Iran

Received: July 2021

Revised: August 2021

Accepted: September 2021

DOI: 10.22068/ijmse.2384

**Abstract:** The main purpose of this investigation was to assess the effect of post-deposition annealing treatment on the electrochemical behavior of TiN coating developed on AISI 304 stainless steel substrate using cathodic arc evaporation physical vapor deposition (CAE-PVD). Post-annealing treatment at 400°C was performed on the coated substrate for 1 h. The studied samples were characterized using X-ray diffraction (XRD), scanning electron microscope (SEM), potentiodynamic polarization (PDP), and electrochemical impedance spectroscopy (EIS) tests. The preferred orientation of TiN (111) was verified by XRD patterns. The crystallinity of the coating was increased after annealing treatment. SEM observations indicated that TiN coatings free of cracks were developed on the substrate. The electrochemical measurements elucidated that the annealed coating had better corrosion resistance compared to that of the as-deposited coating with a lower current corrosion density. This investigation implies that improved corrosion performance of the TiN coating can be achieved by performing post-deposition annealing treatment.

**Keywords:** post-deposition annealing, electrochemical behavior, TiN coating, CAE-PVD, EIS.

## 1. INTRODUCTION

In recent years, among the numerous coatings available on the market, nitride-based coatings such as titanium nitride (TiN) are extensively used to improve the electrochemical, mechanical, and tribological properties of the coated tools. TiN is one of the first transition nitride coatings that has gained a lot of interest from researchers, because of its properties including high corrosion resistance, hardness, and wear resistance, and is deposited on the surfaces of medical implants [1, 2], mechanical, and industrial components [3–6]. In a nutshell, the deposition of TiN results in amelioration of the superficial properties [7–14], the functionality of the parts (electrical, optical, etc.), and esthetical finishing of the components by giving a yellow-gold luster [15–18]. The properties displayed by the nitride coating are attributed to the type of elements, the quantity of the elements, and the deposition parameters used during coating deposition by CAE-PVD [19]. Because of the high deposition rate and good adhesion of the coating to the substrate, the CAE-PVD technique is extensively used to deposit nitride coating. Although this technique is an efficient deposition method, however, it introduces some intrinsic defects which can be detrimental to the functionality of the coatings. In

CAE-PVD, a continuous or pulsed electric current at low voltage is passed between the cathode and anode electrode resulting in the evaporation target material (cathode). The evaporated materials are deposited on the substrates in the form of atoms, molecules, and micro-droplets, and the latter resulting in formation of the macro-particles [20].

The macro-particles can be detached from the surface, leading to the formation of the preferred diffusive paths through the coating to the substrates [21]. During deposition by CAE-PVD, the substrate and the coating materials are heated to a specific temperature. Since the substrate and the coating are made up of different alloys, this phenomenon can cause different thermal coefficients and lattice mismatch between the coatings and the substrates [22]. The difference in the thermal coefficients will result in the formation of residual stress. Certain properties such as adhesion, hardness, and corrosion resistance of the coatings are impressed affected by the residual stresses created during the CAE-PVD process [20, 23]. Although nitride coatings have been proven to have good properties, researchers are still investigating ways to improve the mechanical, tribological, and corrosion resistance of nitride CAE-PVD coatings [24]. Proposals to achieve a superior coating include

finding the optimal deposition parameters during the CAE-PVD process (i.e., arc current, voltage, and temperature) [25], treatment of the substrate before deposition (pre-deposition treatment) [26], treatment of the coatings during deposition (intermediate treatment) [27], and after deposition treatment (post-deposition treatment) [28].

One of the post-deposition treatments on monolayer coatings that has gained a lot of interest in recent years is annealing [12, 29–37]. Hsu et al. [38], by depositing a TiN coating on AISI 316L stainless steel substrate (using CAE-PVD), observed that annealing improved the resistance to pitting corrosion when the samples were immersed in hydrochloric acid and also enhanced the adhesion of the coating. Xi et al. [39], investigated the influence of annealing on the mechanical behavior of TiN coating developed using unbalanced magnetron sputtering, reported that the mechanical properties were enhanced by the annealing treatment. Jafari et al. [40] analyzed the annealing effect on the optical characteristics of TiN. Also, Ponon et al. [41], in the case of annealed TiN deposited by magnetron sputtering, observed a change in the electrical and thermal properties after performing annealing treatment. Popovic et al. [42] examined the effect of annealing TiN on the optical characteristics and agreed with other researchers that annealing treatment affects the functionality of the coating.

Although a lot of research has been done on the effect of post-deposition annealing on titanium nitride coatings, nevertheless, the effect of annealing treatment on the electrochemical properties using PDP and EIS has not been investigated. Therefore, this study aims to investigate the electrochemical behaviors of TiN coating after post-deposition annealing in Ringer's solution. For this purpose, TiN coating was deposited on AISI 304 stainless steel using the CAE-PVD technique and electrochemical behavior evaluated using the aforementioned electrochemical tests.

## 2. MATERIALS AND METHODS

### 2.1. Coating and annealing procedure

In this study, TiN coating was deposited on AISI 304 substrate using the CAE-PVD method (DS&CA601, Yar-Nikan Saleh, Tehran, Iran). The substrates were cleaned with acetone and

alcohol using an ultrasonic cleaner for 20 minutes and subsequently, the ion bombardment process with a bias pulsed-DC voltage of -800 V for 20 minutes by argon gas was applied. TiN alloy was used as the target material with a target current of 120 A was utilized. Then, the coating was conducted under the vacuum pressure of  $5 \times 10^{-5}$  torr. During the deposition process, the distance between the substrate and the target was 15 cm under temperature of 200°C. The rotation speed for the samples were set at 5 r.p.m with a deposition time of 90 minutes. It should be mentioned that a Ti interlayer was deposited between TiN coating and the substrate to achieve good adhesion of TiN coating [43]. The samples were placed in an air furnace and heated at 10°C/min until the temperature reached 400°C. Finally, annealing treatment was performed for 1 h, then cooled to room temperature inside the furnace.

### 2.2. Surface Characterization

The surface morphology of as-deposited and post-annealed coated specimens was measured by an scanning electronic microscope (SEM) (JEOL, JSM-840A, Tokyo, Japan). The thickness of the coating was analyzed using field emission scanning electron microscopy (FESEM) (MIRA TESCAN, Brno –Kohoutovice, Czech Republic). The present phases and crystallographic structures were clarified using an X-ray diffractometer (XRD) (Philips -PW1730, Eindhoven, Netherlands) equipped with beam monochromator copper target ( $K_{\alpha}$  radiation at 30 mA and 40000 V) and a scanning angular ranging from 10 to 80° with a scanning rate of 0.05° and a 1 s step size. Panalytical X'Pert high score plus software was used to quantify the present phases and calculate the crystallite size of the samples using Scherrer's equation. The adhesion of the coatings was investigated using Rockwell-C hardness (HRC) according to VDI 3198 by applying a force of 1471 N for 30 seconds [44].

### 2.3. Electrochemical measurements

The electrochemical behavior of the specimens was examined in Ringer's solution using the autolab type III/FRA2 system conducting Nova software 1.7. The electrochemical tests (PDP and EIS measurements) were performed under an aerated condition in a three-electrode flat cell containing a Pt counter electrode, an Ag/AgCl

reference electrode, and the studied samples as working electrodes. Before performing the test, the specimens were immersed in the Ringer's solution under the open circuit potential (OCP) condition to reach stability. Then, by applying a starting potential of  $-250 \text{ mV}_{\text{Ag/AgCl}}$  versus the stabilized OCP to  $1.8 \text{ V}_{\text{Ag/AgCl}}$ , the PDP tests were carried out with the scanning rate of  $1 \text{ mV/s}$ . The electrochemical impedance spectroscopy tests were conducted in the frequency range of  $100 \text{ kHz}$  to  $10 \text{ mHz}$ . The amplitude of the sinusoidal AC voltage employed in EIS measurements was  $5 \text{ mV}$ .

### 3. RESULTS AND DISCUSSION

#### 3.1. Microstructural characterization

The surface and the cross-sectional morphology of TiN coated samples including as-deposited and annealed specimens were indicated in Fig. 1. As shown in Fig. 1, the morphology of the surface showed the typical cathodic arc deposited coating

features, including micropores and macroparticles distributed on the surface of the coating [20].

As can be seen in Fig. 2, the patterns of XRD reveal the presence of TiN (NaCl structure) and Ti (hexagonal close-packed) peaks in as-deposited and annealed coatings (JCPDS no.38-1420) [45], similar patterns for TiN coatings deposited by CAE-PVD were reported by other researchers [46]. Scherrer's equation (Eq. 1) was utilized to calculate the crystalline size ( $D$ ) of the as-deposited and annealed specimens as follows [47–50]:

$$D = \frac{b\lambda}{\beta \cos \theta} \quad (1)$$

Where,  $b$  is the Scherrer's constant which, is equal to  $0.9$ ,  $\beta$  represents full width at half maximum (FWHM) of each peak,  $\lambda$  is the wavelength ( $=0.154 \text{ nm}$ ), and  $\theta$  is the diffraction angle. As reported in Table 1, the crystallite size increased from  $12$  to  $20 \text{ nm}$  after post-deposition annealing treatment [40, 42].



Fig. 1. SEM images of the surface and cross-sectional (a, b) as-deposited and (c) annealed specimens.

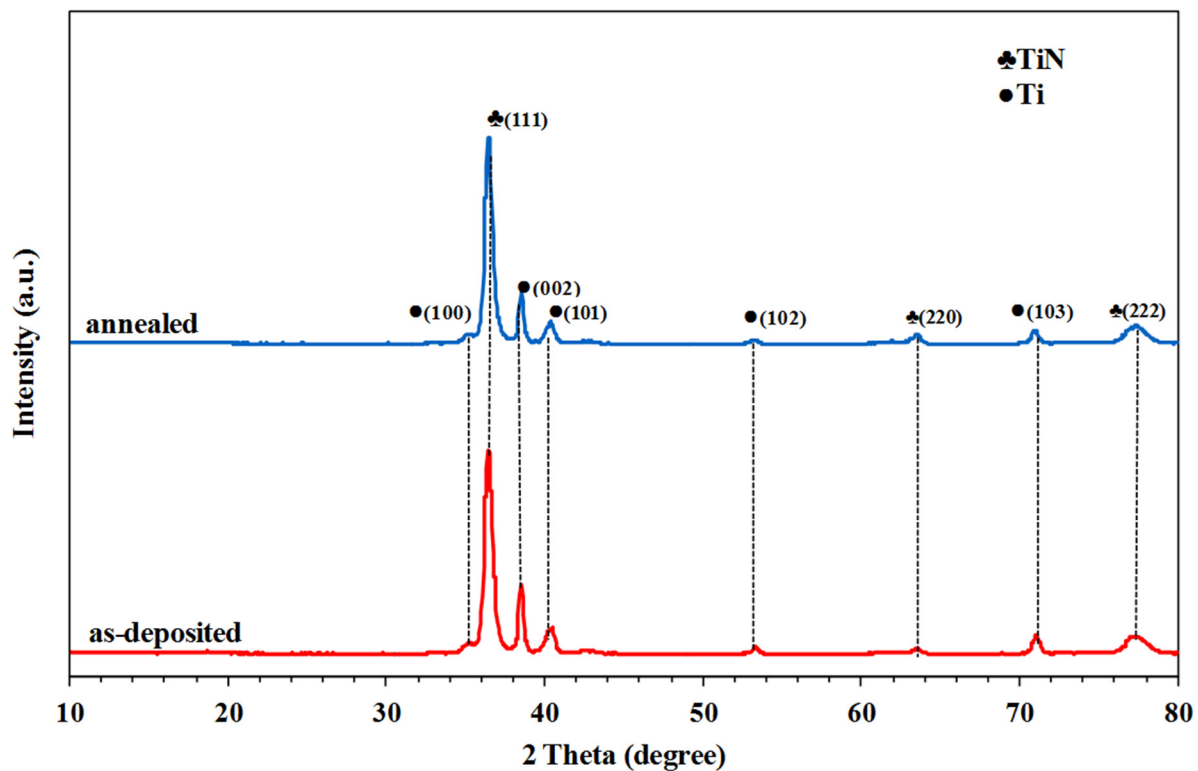


Fig. 2. XRD patterns of as-deposited and annealed specimens.

**Table 1.** Crystallite size, microstrain, and dislocation density values of as-deposited and annealed specimens

| Sample           | Crystallite size (nm) | Dislocation density ( $10^{-15}$ line/m <sup>2</sup> ) | Macro strain ( $10^{-3}$ ) |
|------------------|-----------------------|--|----------------------------|
| As-deposited     | 12                    | 6.9  | 7.98                       |
| Annealed (400°C) | 20                    | 2.5  | 5.79                       |

This phenomenon can be due to the increase in the kinetic energy and reconfiguration of the atoms as a result of the grain boundary migration and sub-grain growth during annealing treatment [42]. The microstrain ( $\epsilon$ ) was calculated using the formula below (Eq. 2):

$$\epsilon = \frac{\beta}{4 \tan \theta} \quad (2)$$

Williamson and Smallman's equation (Eq. 3) was used to determine the dislocation density ( $\delta$ ) of the as-deposited and annealed specimens.

$$\delta = \frac{1}{D^2} \quad (3)$$

The values of the dislocation density and the microstrain were presented in Table 1. Considering Table 1, dislocation density and microstrain decreased after annealing treatment. This can be attributed to the increase in crystallinity and annihilation of defects [51, 52].

### 3.2. Adhesion tests

As mentioned before, the quality of adhesion of the coatings was evaluated based on VDI 3198 indentation test [44]. In the present study, the surface of the samples has been loaded with a Rockwell-C indenter and the vestiges of the indenter evaluated using optical microscope (OM) images (Fig. 3).

Considering Fig. 3, no vestiges of delamination and cracks (correspond to HF1 class adhesion) were displayed by both coatings. It can be noted that the effect of annealing treatment on the adhesion of the TiN coatings is inappreciable [38].

### 3.3. Electrochemical analysis

The Nyquist and Bode plots of as-deposited and annealed specimens after an immersion time of 24 and 168 h in Ringer's solution under OCP conditions were displayed in Fig. 4.





Fig. 3. Images of Rockwell-C indentations for adhesion of (a) as-deposited and (b) annealed specimens.

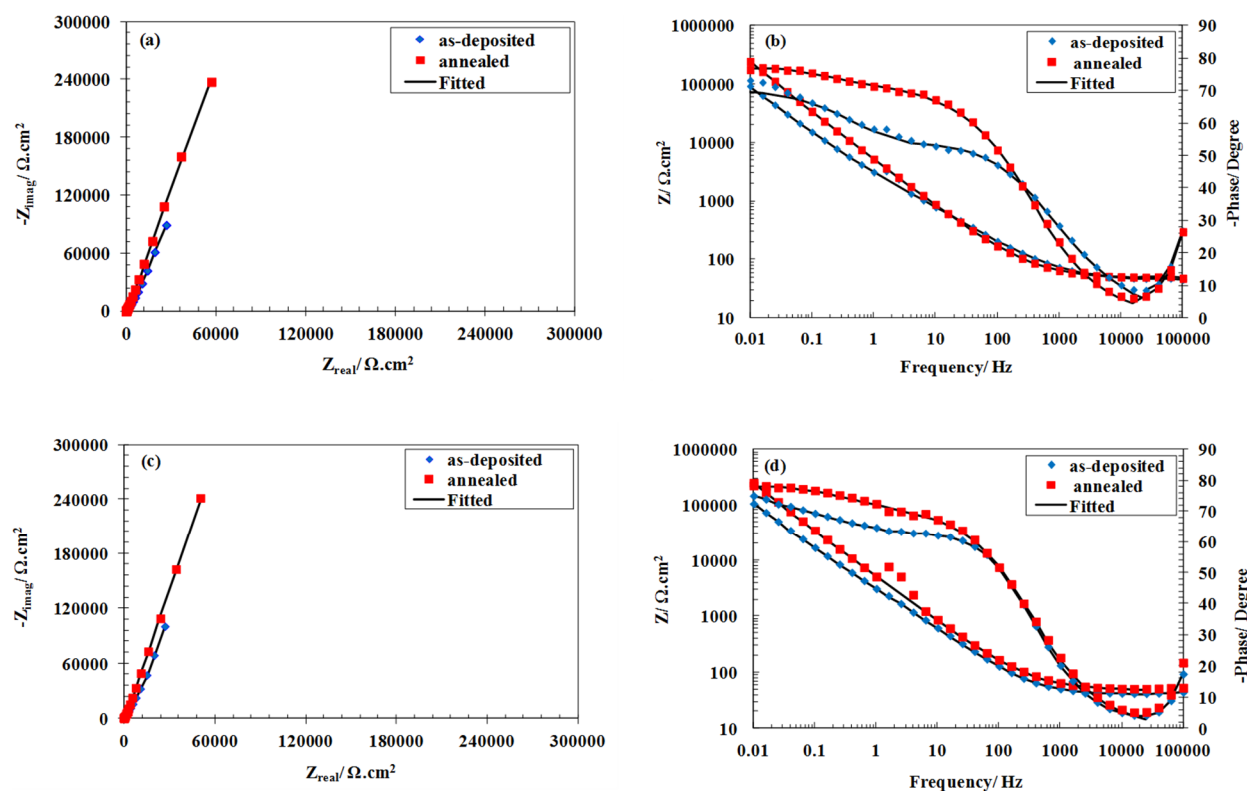


Fig. 4. (a, c) Nyquist and (b, d) Bode curves of as-deposited and annealed specimens at OCP condition.

As can be seen in the Nyquist plots of Fig. 4 (a and c), by annealing treatment, the polarization resistance of the coating increased. Also, the diameter of the semi-circles of the studied samples increased by immersion time, implying that the corrosion resistance was enhanced [53, 54]. Considering the Bode phase plots of Fig. 4 (b and d), it is clear that the maximum phase angles

(MPAs) are lower than  $90^\circ$ . This behavior is ascribed to the non-ideal capacitor or constant phase element (CPE). Therefore, it is necessary to use CPE for fitting and simulating the experimental EIS data [54]. It is reported that the presence of CPE in CAE-PVD coatings is due to the surface heterogeneity of the coating as a result of macroparticles and micropores [55]. The

impedance of CPE can be expressed as follows [24]:

$$Z = \frac{1}{Q(j\omega)^\alpha} \quad (4)$$

where  $Q$  signifies the CPE constant,  $j$  is the imaginary number ( $J^2 = -1$ ),  $\omega$  represents the angular frequency (in radian per second), and  $\alpha$  accounts for frequency-dependent parameter which varies with the surface roughness and defects present on the surface of the coating [35]. The validation of the experimental EIS tests is dependent on the stability of the electrochemical system during recording EIS spectra. Therefore, the EIS system should fulfill three requirements of linear system theory (LST) including causality, stability, and linearity.

Failure to fulfill these triple requirements discredits the EIS data [56]. For this purpose (reliability of EIS data), it is common to use Kramers-Kronig transformations (KKTs). The KKTs were employed on the experimental EIS data by transforming the imaginary ( $Z'$ ) and the real ( $Z''$ ) axes to the real and the imaginary axes, respectively, to compare and contrast the obtained transformed quantities and the experimental EIS

data. As shown in Fig. 5, the experimental EIS data and transformed results overlapped one another that accredits the validation of the recorded experimental EIS data [53]. In this study, the electrical equivalent circuit (EEC), characterized by two-time constants, as illustrated in Fig. 4 [57]. The same EEC has been employed by other researchers to fit and simulate experimental EIS data for mono and multilayer nitride coatings [24, 55, 58–60]. In Fig. 6,  $R_s$  signifies the solution resistance,  $R_{por}$  denotes the coating resistance due to the presence of pores, and  $R_{ct}$  accounts for the charge transfer resistance between the coating and the substrate interface,  $CPE_{por}$  and  $CPE_{dl}$  are representative of the capacitance of the coating and the double layer capacitance, respectively [57]. The electrical parameters obtained by fitting the experimental data according to EEC shown in Fig. 6, were summarized in Table 2. According to the presented data,  $R_p$  for the annealed coating was greater than that of the as-deposited coating for both immersion times. In addition, for each sample, the corrosion resistance increased as the immersion time increased.



**Fig. 5.** KKTs of the EIS data acquired for (a, b) as-deposited and (c, d) annealed specimens after (a, c) 24 h and (b, d) 168 h of stabilization in Ringer's solution.

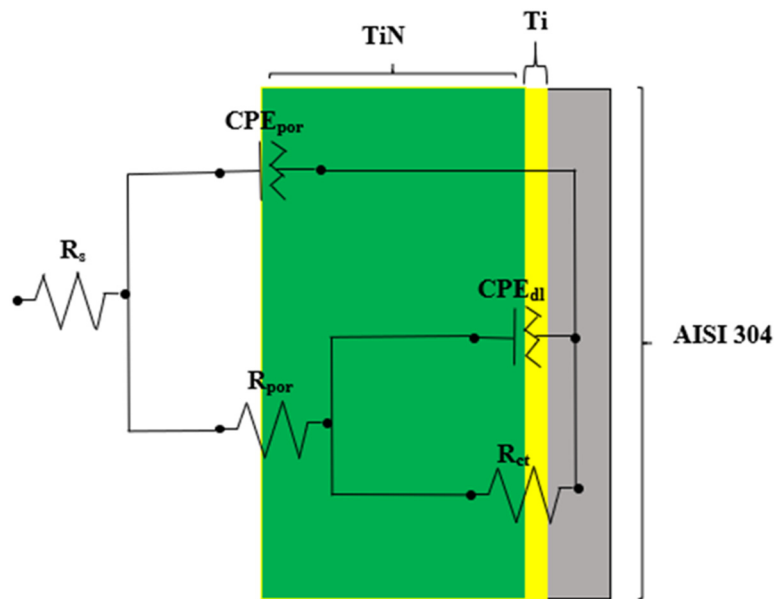


Fig. 6. EEC for fitting experimental EIS data of as-deposited and annealed specimens.

Table 2. EIS parameters of as-deposited and annealed specimens according to immersion time in Ringer's electrolyte acquired by EEC simulation.

| Sample           | Immersion time (h) | $R_s$ ( $\Omega \cdot \text{cm}^2$ ) | $R_{por}$ ( $\text{k}\Omega \cdot \text{cm}^2$ ) | $CPE_{por}$ ( $\times 10^{-4} \text{S}^n / \Omega \cdot \text{cm}^2$ ) | $n_1$ | $R_{ct}$ ( $\text{M}\Omega \cdot \text{cm}^2$ ) | $CPE_{dl}$ ( $\times 10^{-4} \text{S}^n / \Omega \cdot \text{cm}^2$ ) | $n_2$ | $R_p$ | $\chi^2$ |
|------------------|--------------------|--------------------------------------|--|--|-------|---|---|-------|-------|----------|
| As-deposited     | 24                 | 113                                  | 2.10   | 0.75   | 0.88  | 3.3   | 0.021   | 0.97  | 3.3   | 0.001    |
|                  | 168                | 112                                  | 2.13   | 0.68   | 0.88  | 19.1  | 0.035   | 0.88  | 19.1  | 0.001    |
| Annealed (400°C) | 24                 | 111                                  | 2.10   | 0.61   | 0.87  | 86.9  | 0.090   | 0.90  | 86.9  | 0.005    |
|                  | 168                | 112                                  | 2.30   | 0.53   | 0.88  | 173.0   | 0.079   | 0.87  | 173.0 | 0.002    |

Fig. 7 displays the PDP curves of as-deposited and annealed specimens after 168 h immersion in Ringer's solution. Tafel extrapolation was used to calculate the corrosion potential and the current density and the obtained results were summarized in Table 3.

Table 3. PDP data of as-deposited and annealed specimens according to immersion time in Ringer's electrolyte.

| Sample           | $E_{corr}$ (mV) | $i_{corr}$ ( $\mu\text{A} \cdot \text{cm}^{-2}$ ) |
|------------------|-----------------|---|
| As-deposited     | -6.5            | 0.014   |
| Annealed (400°C) | -38.0           | 0.013   |

The annealed sample exhibited a higher corrosion potential of -38 mV and a lower current corrosion density ( $0.013 \mu\text{A} \cdot \text{cm}^{-2}$ ) than that of the as-deposited sample. The results from the PDP are in good agreement with the EIS results, represent that post-deposition annealing improved the resistance of the coating.

According to the aforementioned results the

difference in the electrochemical behavior of as-deposited and annealed samples can be ascribed to the change in the defects on the surface [61], relaxation of stress [62], and probable  $\text{TiO}_2$  formation [38].

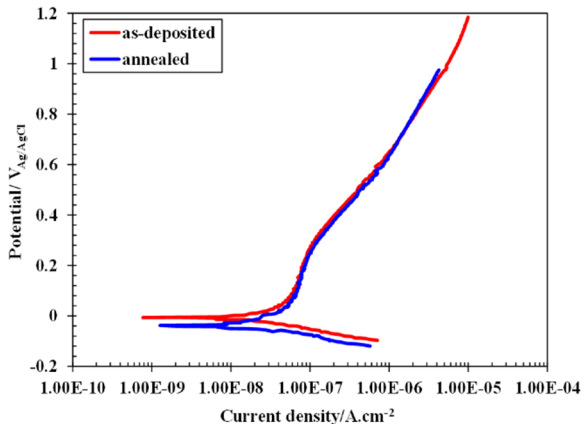


Fig. 7. PDP curves of (a) as-deposited and (b) annealed specimens in Ringer's solution.

The decrease in the porosity due to the grains growth kinetics and vacancy diffusion model

reduces the possible infiltration path of the solute [63]. Furthermore, the densification of the coating increased the corrosion resistance [64]. In addition, the increase in crystallite size effectively reduced the grain boundary area and decreased corrosion initiation sites [65]. SEM observations were performed to compare the surface of the coating before and after the electrochemical test. As shown in Fig. 8, there was no evidence of pitting, crevice, or galvanic corrosion on the surface of as-deposited and annealed samples. Therefore, the annealed coating is durable for a long time when exposed to Ringer's solution.



**Fig. 8.** Surface SEM images of (a) as-deposited and (b) annealed specimens after electrochemical analysis in Ringer's solution.

#### 4. CONCLUSIONS

This study aimed to investigate the effects of the post-annealing treatment on TiN coating. The post-deposition annealing treatment was conducted at 400°C. TiN coating was deposited on AISI 304 substrate using the CAE-PVD

method. The surface morphology of the as-deposited and annealed coating showed the presence of macroparticles and pinhole distributed on the surface of the coatings. The XRD analysis showed the presence of TiN and Ti phases with NaCl and hexagonal structure, respectively. Due to the thermal treatment, dislocations density in the coating decreased resulting in the decrease in microstrain. The quality of the coating was satisfactory as there were no cracks or areas of delamination after the adhesion test. The crystallite size increased as a result of annealing treatment. KKT transformation confirmed the validity of the obtained data according to LST theory. The electrochemical tests indicated that annealed coatings had better corrosion resistance with an increase of 9% and had more protective properties than that of as-deposited coatings, which was primarily due to the decrease in porosity, increase in the grain size which decreased the active anodic area. In a nutshell, the results indicates that the annealing treatment can improve the electrochemical performance of TiN coating in Ringer's solution and decrease the microstrain without compromising the integrity of the coating.

#### 5. REFERENCES

- [1] Uddin, G. M., Jawad, M., Ghufraan, M., Saleem, M. W., Raza, M. A., Rehman, Z. U., Arafat, S. M., Irfan, M., Waseem, B., "Experimental investigation of tribo-mechanical and chemical properties of TiN PVD coating on titanium substrate for biomedical implants manufacturing." *Int. J. Adv. Manuf. Technol.* 2019, 102, 1391–1404.
- [2] Hussein, M. A., Anka, N. K., Kumar, A. M., Azeem, M. A., Saravanan, S., Sorour, A. A., Aqeeli, N. Al, "Mechanical, biocorrosion, and antibacterial properties of nanocrystalline TiN coating for orthopedic applications." *Ceram. Int.* 2020, 46, 18573–18583.
- [3] Elmkhah, H., Abdollah-zadeh, A., Mahboubi, F., Rouhaghdam, A. R. S., Fattah-alhosseini, A., "Correlation between the duty cycle and the surface characteristics for the nanostructured titanium aluminum nitride coating



- deposited by pulsed-DC PACVD technique.” *J. Alloys Compd.* 2017, 711, 530–540.
- [4] Jokar, K., Elmkhah, H., Fattah-alhosseini, A., Babaei, K., Zolriasatein, A., “Comparison of the wear and corrosion behavior between CrN and AlCrN coatings deposited by Arc-PVD method.” *Mater. Res. Express* 2019, 6, 116426.
- [5] Sahib Mansoor, N., Fattah-alhosseini, A., Shishehian, A., Elmkahah, H., “Tribological properties of different types of coating materials deposited by cathodic arc-evaporation method on Ni-Cr dental alloy.” *Mater. Res. Express* 2019, 6, 056421.
- [6] Mansoor, N. S., Fattah-alhosseini, A., Elmkhah, H., Shishehian, A., “Comparison of the mechanical properties and electrochemical behavior of TiN and CrN single-layer and CrN/TiN multi-layer coatings deposited by PVD method on a dental alloy.” *Mater. Res. Express* 2020, 6, 126433.
- [7] Naghibi, S. A., Raeissi, K., Fathi, M. H., “Corrosion and tribocorrosion behavior of Ti/TiN PVD coating on 316L stainless steel substrate in Ringer’s solution.” *Mater. Chem. Phys.* 2014, 148, 614–623.
- [8] Qin, Y., Xiong, D., Li, J., “Surface & Coatings Technology Tribological properties of laser surface textured and plasma electrolytic oxidation duplex-treated Ti6Al4V alloy deposited with MoS<sub>2</sub> film.” *Surf. Coat. Technol.* 2015, 269, 266–272.
- [9] Teles, V. C., Mello, J. D. B. De, Silva, W. M., “Abrasive wear of multilayered / gradient CrAlSiN PVD coatings : Effect of interface roughness and of superficial flaws.” *Wear* 2017, 376–377, 1691–1701.
- [10] Hoche, H., Groß, S., Troßmann, T., Schmidt, J., Oechsner, M., “PVD coating and substrate pretreatment concepts for magnesium alloys by multinary coatings based on Ti (X) N.” *Surf. Coat. Technol.* 2013, 228, 336–341.
- [11] Ramoul, C., Beliardouh, N. E., Bahi, R., Nouveau, C., Djahoudi, A., Walock, M. J., Michael, J., Ramoul, C., “Surface performances of PVD ZrN coatings in biological environments.” *Tribol. - Mater. Surfaces Interfaces* 2018, 13, 1–8.
- [12] Chen, W., Meng, X., Wu, D., Yao, D., Zhang, D., “The effect of vacuum annealing on microstructure, adhesion strength and electrochemical behaviors of multilayered AlCrTiSiN coatings.” *Appl. Surf. Sci.* 2019, 467–468, 391–401.
- [13] Chen, X., Pang, X., Meng, J., Yang, H., “Thermal-induced blister cracking behavior of annealed sandwich-structured TiN/CrAlN films.” *Ceram. Int.* 2018, 44, 5874–5879.
- [14] Mani, S. P., Rikhari, B., Agilan, P., Rajendran, N., “Evaluation of the corrosion behavior of a electrochemical impedance spectroscopy.” 2018, DOI: 10.1039/c8nj01649f.
- [15] Łępicka, M., Grądzka-Dahlke, M., Pieniak, D., Pasierbiewicz, K., Kryńska, K., Niewczas, A., “Tribological performance of titanium nitride coatings: A comparative study on TiN-coated stainless steel and titanium alloy.” *Wear* 2019, 422–423, 68–80.
- [16] Sunthornpan, N., Watanabe, S., Moolsradoo, N., “Corrosion resistance and cytotoxicity studies of DLC, TiN and TiCN films coated on 316L stainless steel.” *J. Phys. Conf. Ser.* 2018, 1144, 012013.
- [17] Dalibon, E. L., Cabo, A., Halabi, J., Moreira, R. D., Silva, K., Brühl, S. P., “Mechanical and Corrosion Behavior of TiN Coatings Deposited on Nitrided AISI 420 Stainless Steel.” 2019, 813, 135–140.
- [18] Martinho, R. P., Silva, F. J. G., Martins, C., Lopes, H., “Comparative study of PVD and CVD cutting tools performance in milling of duplex stainless steel.” *Int. J. Adv. Manuf. Technol.* 2019, 102, 2423–2424.
- [19] Johnson, L. J. S., Rogström, L., Johansson, M. P., Odén, M., Hultman, L., “Microstructure evolution and age hardening in (Ti, Si) (C, N) thin films deposited by cathodic arc evaporation.” *Thin Solid Films* 2010, 519, 1397–1403.
- [20] Mattox, D. M., *Handbook of Physical Vapor Deposition (PVD) Processing.* Elsevier 2010.
- [21] Panjan, P., Cekada, M., Panjan, M., “Growth defects in PVD hard coatings.” *Vacuum* 2010, 84, 209–214.
- [22] Abadías, G., Chason, E., Keckes, J.,

- Sebastiani, M., Thompson, G. B., Barthel, E., Doll, G. L., Murray, C. E., Stoessel, C. H., Martinu, L., "Stress in thin films and coatings : Current status , challenges , and prospects." *Vacuum* 2019, 020801, DOI: 10.1116/1.5011790.
- [23] Skordaris, G., Bouzakis, K. D., Kotsanis, T., Charalampous, P., "Effect of PVD film's residual stresses on their mechanical properties, brittleness, adhesion and cutting performance of coated tools." *CIRP J. Manuf. Sci. Technol.* 2016, 05, 5–11.
- [24] Mohamadian Samim, P., Fattah-alhosseini, A., Elmkhah, H., Imantalab, O., "A study on the corrosion resistance of ZrN/CrN multilayer nanostructured coating applied on AISI 304 stainless steel using Arc-PVD method in 3.5 wt% NaCl solution." *Mater. Res. Express* 2019, 6, 126426.
- [25] Maksakova, O., Simo, S., Pogrebnyak, A., Bondar, O., Kravchenko, Y., Beresnev, V., Erdybaeva, N., "The influence of deposition conditions and bilayer thickness on physical- mechanical properties of CA-PVD multilayer ZrN/CrN coatings." *Mater. Charact.* 2018, 140, 189–196.
- [26] Felmetsger, V. V., Mikhov, M. K., Laptev, P. N., "Effect of Pre-Deposition RF Plasma Etching on Wafer Surface Morphology and Crystal Orientation of Piezoelectric AlN Thin Films." *IEEE* 2015, 62, 387–391.
- [27] Abusuilik, S. B., Inoue, K., "Effects of intermediate surface treatments on corrosion resistance of cathodic arc PVD hard coatings." *Surf. Coat. Technol.* 2013, 237, 421–428.
- [28] Abusuilik, S. B., "Pre-, intermediate, and post-treatment of hard coatings to improve their performance for forming and cutting tools." *Surf. Coat. Technol.* 2015, 284, 384–395.
- [29] Dong, Y., Yang, Y., Chu, Z., Zhang, J., He, J., Yan, D., Li, D., "Effect of annealing in Ar on the microstructure and properties of thick nano-grained TiN ceramic coatings." *Ceram. Int.* 2017, 43, 9303–9309.
- [30] Hahn, R., Bartosik, M., Arndt, M., Polcik, P., Mayrhofer, P. H., "Annealing effect on the fracture toughness of CrN/TiN superlattices." *Int. J. Refract. Met. Hard Mater.* 2018, 71, 352–356.
- [31] Kim, J., Jeong, G. Y., Kim, S., Jeong, Y. J., Sohn, D., "Effect of coating thickness and annealing temperature on ZrN coating failure of U-Mo particles under heat treatment." *J. Nucl. Mater.* 2018, 507, 347–359.
- [32] Liu, X., Iamvasant, C., Liu, C., Matthews, A., Leyland, A., "CrCuAgN PVD nanocomposite coatings: Effects of annealing on coating morphology and nanostructure." *Appl. Surf. Sci.* 2017, 392, 732–746.
- [33] Liu, X., Tao, X., Liu, C., Matthews, A., Leyland, A., "Investigation of the nanostructure of as-deposited and post-coat annealed CrCuAgN PVD nanocomposite coatings." *Mater. Chem. Phys.* 2020, 255, 123499.
- [34] Babincová, P., Sahul, M., Drobný, P., Č, L., "Morphological changes of the PVD coatings after isothermal annealing Morphological changes of the PVD coatings after isothermal annealing." 2020, DOI: 10.1088/1757-899X/726/1/012001.
- [35] Adesina, A. Y., "Electrochemical evaluation of the corrosion protectiveness and porosity of vacuum annealed CrAlN and TiAlN cathodic arc physical vapor deposited coatings." *Mater. Corros.* 2019, DOI: 10.1002/maco.201810715.
- [36] Chen, M., Cai, F., Chen, W., Wang, Q., Zhang, S., "Influence of vacuum annealing on structures and properties of AlTiSiN coatings with corrosion resistance." *Surf. Coat. Technol.* 2017, 312, 25–31.
- [37] Chen, W., Yan, A., Meng, X., Wu, D., Yao, D., Zhang, D., "Microstructural change and phase transformation in each individual layer of a nano-multilayered AlCrTiSiN high-entropy alloy nitride coating upon annealing." *Appl. Surf. Sci.* 2018, 462, 1017–1028.
- [38] Hsu, C., Liu, H., Huang, W., Lin, M., "Effect of Post Heated TiN Coating on Pitting Corrosion of Austenitic Stainless Steel." *J. Coat. Sci. Technol.* 2016, 2, 93–99.
- [39] Xi, Y., Fan, H., Liu, W., "The effect of annealing treatment on microstructure and properties of TiN films prepared by unbalanced magnetron sputtering." *J. Alloys Compd.* 2010, 496, 695–698.
- [40] Jafari, A., Ghoranneviss, Z., Elahi, A. S.,

- Ghoranneviss, M., Fasihi Yazdi, N., Rezaei, A., "Effects of Annealing on TiN Thin Film Growth by DC Magnetron Sputtering." *Adv. Mech. Eng.* 2014, 2014, DOI: 10.1155/2014/373847.
- [41] Ponon, N. K., Appleby, D. J. R., Arac, E., King, P. J., Ganti, S., Kwa, K. S. K., O'Neill, A., "Effect of deposition conditions and post deposition anneal on reactively sputtered titanium nitride thin films." *Thin Solid Films* 2015, 578, 31–37.
- [42] Popovi, M., Novakovi, M., Popovic, M., Novakovic, M., Bibic, N., "Annealing effects on the properties of TiN thin films." *Process. Appl. Ceram.* 2015, 9, 67–71.
- [43] Ali, R., Sebastiani, M., Bemporad, E., "Influence of Ti-TiN multilayer PVD-coatings design on residual stresses and adhesion." *Mater. Des.* 2015, 75, 47–56.
- [44] Vidakis, N., Antoniadis, A., Bilalis, N., "The VDI 3198 indentation test evaluation of a reliable qualitative control for layered compounds." *J. Mater. Process. Technol.* 2003, 143–144, 481–485.
- [45] Matei, A. A., Pencea, I., Stanciu, S. G., Hristu, R., Antoniac, I., Ciovica, E., Sfât, C. E., Stanciu, G. A., "Structural characterization and adhesion appraisal of TiN and TiCN coatings deposited by CAE-PVD technique on a new carbide composite cutting tool." *J. Adhes. Sci. Technol.* 2015, 29, 2576–2589.
- [46] Wu, Y.-P., Li, Z.-Y., Zhu, S., Lu, L., Cai, Z.-B., "Effect of frequency on fretting wear behavior of Ti / TiN multilayer film on depleted uranium." *Trans. Nonferrous Met. Soc. China* 2017, 12, 1–11.
- [47] Attarzadeh, F. R., Elmkhah, H., Fattah-Alhosseini, A., "Comparison of the Electrochemical Behavior of Ti and Nanostructured Ti-Coated AISI 304 Stainless Steel in Strongly Acidic Solutions." *Metall. Mater. Trans. B* 2017, 48, 227–236.
- [48] Fattah-alhosseini, A., Elmkhah, H., Attarzadeh, F. R., "On the Electrochemical Behavior of PVD Ti-Coated AISI 304 Stainless Steel in Borate Buffer Solution." *J. Mater. Eng. Perform.* 2017, 26, 1792–1800.
- [49] Elmkhah, H., Attarzadeh, F., Fattah-alhosseini, A., Kim, K. H., "Microstructural and electrochemical comparison between TiN coatings deposited through HIPIMS and DCMS techniques." *J. Alloys Compd.* 2018, 735, 422–429.
- [50] Elmkhah, H., Fattah-alhosseini, A., Babaei, K., Abdollah-Zadeh, A., Mahboubi, F., "Correlation between the Al content and corrosion resistance of TiAlN coatings applied using a PACVD technique." *J. Asian Ceram. Soc.* 2020, 8, 72–80.
- [51] Anwar, S., Anwar, S., "Thermal stability studies of tungsten nitride thin." *Surf. Eng.* 2016, 33, 276–281.
- [52] Hojabri, A., Hajakbari, F., "Annealing temperature effect on the properties of untreated and treated copper films with oxygen plasma." *J. Theor. Appl. Phys.* 2014, 8, 1–7.
- [53] Fattah-alhosseini, A., Imantalab, O., "Enhancing the Electrochemical Behavior of Pure Copper by Cyclic Potentiodynamic Passivation: A Comparison between Coarse- and Nano-Grained Pure Copper." *Metall. Mater. Trans. B* 2016, 47, 2761–2770.
- [54] Fattah -alhosseini, A., Imantalab, O., "Effect of accumulative roll bonding process on the electrochemical behavior of pure copper." *J. Alloy Compd.* 2015, 632, 48–52.
- [55] Samim, P. M., Fattah-alhosseini, A., Elmkhah, H., Imantalab, O., Nouri, M., "A study on comparing surface characterization and electrochemical properties of single-layer CrN coating with nanostructured multilayer ZrN/CrN coating in 3.5 wt.% NaCl solution." *Surfaces and Interfaces* 2020, 21, 100721.
- [56] Omid, S., Fattah-alhosseini, A., Mazaheri, Y., "Effect of grain refinement on mechanical and electrochemical properties of ultra-fine grained AA1050 fabricated via ARB process." *J. Manuf. Process.* 2016, 22, 269–277.
- [57] Çaha, I., Alves, A. C., A, L. J., Lisboa-filho, P. N., Silva, J. H. D., Rocha, L. A., Pinto, A. M. P., Toptan, F., "Corrosion and tribocorrosion behaviour of titanium nitride thin films grown on titanium under different deposition times." *Surf. Coat.*

- Technol. 2019, 374, 878–888.
- [58] Mohamadian Samim, P., Fattah-Alhosseini, A., Elmkhah, H., Imantalab, O., “Structure and corrosion behavior of ZrN/CrN nano-multilayer coating deposited on AISI 304 stainless steel by CAE-PVD technique.” *J. Asian Ceram. Soc.* 2020, 8, 460–469.
  - [59] Sahib Mansoor, N., Fattah-alhosseini, A., Shishehian, A., Elmkhah, H., “Corrosion Behavior of Single and Multilayer Coatings Deposited on Ni-Cr Dental Alloy by CAE-PVD Technique.” *Anal. Bioanal. Electrochem.* 2019, 11, 304–320.
  - [60] Wang, L., Wang, M., Chen, H., “Corrosion mechanism investigation of TiAlN/CrN superlattice coating by multi-arc ion plating in 3.5 wt% NaCl solution.” *Surf. Coatings Technol.* 2020, 391, 125660.
  - [61] Chen, M., Cai, F., Chen, W., Wang, Q., Zhang, S., “Influence of vacuum annealing on structures and properties of Al-Ti -Si-N coatings with corrosion resistance.” *Surf. Coat. Technol.* 2016, DOI: 10.1016/j.surfcoat.2016.08.006.
  - [62] Ahmed, M. S., Munroe, P., Jiang, Z. T., Zhao, X., Rickard, W., Zhou, Z. feng, Li, L. K. Y., Xie, Z., “Corrosion behaviour of nanocomposite TiSiN coatings on steel substrates.” *Corros. Sci.* 2011, 53, 3678–3687.
  - [63] Veshchunov, M. S., “Modelling of grain growth kinetics in porous ceramic materials under normal and irradiation conditions.” *Materials (Basel).* 2009, 2, 1252–1287.
  - [64] Krishna, L. R., Purnima, A. S., Sundararajan, G., “A comparative study of tribological behavior of microarc oxidation and hard-anodized coatings.” 2006, 261, 1095–1101.
  - [65] Abd El-Rahman, A. M., “Synthesis and annealing effects on the properties of nanostructured Ti-Al-V-N coatings deposited by plasma enhanced magnetron sputtering.” *Mater. Chem. Phys.* 2015, 149, 179–187.